

SEISMOLOGICAL IMPLICATIONS OF THE GROUND MOTION DATA FROM THE 2003 SAN SIMEON EARTHQUAKE

Vladimir Graizer
California Geological Survey, Strong Motion Instrumentation Program

Douglas Dreger
University of California, Berkeley Seismological Laboratory

Abstract

The San Simeon earthquake occurred on a previously unknown blind thrust fault. No surface rupture associated with the earthquake has been identified. It was recorded at more than 100 strong motion stations out to distances of over 300 km with relatively few stations at less than 50 km distance. The biggest acceleration of 0.48 g was recorded at the Templeton hospital 38 km SE of the epicenter. Data demonstrates strong directivity effect in the direction of rupture propagation. Combined inversion of GPS and seismic waveform data allowed constructing a finite-source model of the earthquake.

Introduction

The M_w 6.5 San Simeon earthquake occurred in central California on December 22 2003 at 11:15:56 a.m. local time. The epicenter was located 7 miles northeast of the town of San Simeon (Hardebeck et al., 2004). The San Simeon earthquake occurred on a reverse fault striking northwest and most likely dipping to the northeast. Earthquake parameters as reported by the California Integrated Seismic Network (CISN) are shown in Table 1.

Table 1. Earthquake Epicenter Information from CISN

Date & Time (Local):	2003/12/22 11:15:56 (PST)
Date & Time (UTC):	2003/12/22 19:15:56 (UTC)
Location:	35.71N 121.10W 7 miles (11 km) NE of San Simeon and 24 miles (39 km) WNW of Paso Robles
Depth (km):	7.5
Magnitude:	6.5 M_w
Mechanism:	Reverse Fault

The earthquake was followed by an active aftershock sequence. Location of the epicenter of the mainshock and aftershocks distribution show that the earthquake most likely ruptured on a

previously unknown blind thrust fault northeast of the Oceanic fault (Jennings, 1994; Hauksson and Oppenheimer, 2004).

The San Simeon area was searched for signs of surface rupture due to earthquake. No features that could be associated with coseismic surface faulting were found. Almost all the earthquake ground effects that were observed are best ascribed to rockfalls, landslides and liquefaction or to the settlement or slumping of man made fills (Hardebeck et al., 2004; Treiman et al., 2004).

Strong Ground Motion

The first automatic CISN ShakeMap was posted on the web 8 minutes after the event based on only 29 stations contributing (Gee et al., 2004). The distribution of CISN strong motion stations in the area is shown in Fig.1. It clearly demonstrates the fact that there are not enough digital stations in the area. The updated versions of the instrumental intensity and peak ground acceleration maps are shown in Fig. 2 and 3.

Strong-motion data for engineering applications after major earthquakes are distributed via the Internet Quick Report (IQR) through the CISN Engineering Data Center. San Simeon earthquake strong-motion data recorded by modern digital instruments were made available through the CISN Engineering Data Center at <http://www.cisn-edc.org> on the day of earthquake (Fig. 4).

The San Simeon earthquake was recorded at more than 100 strong motion stations out to distances of over 300 km, though with relatively few stations at less than 50 km distance. The Internet Quick Report lists the 98 records recovered so far and their peak values and distances. It also provides links to station information, and allows downloading digital data. Many of strong motion stations that recorded this earthquake are the early film recorders, and the films have been developed and scaled. For film records, only peak acceleration is listed. The film records from the three stations (San Antonio Dam, Lopez Lake, and Point Bouchon) have already been digitized and processed, and made available for view and download through the IQR.

The three stations closest to the epicenter recorded peak ground accelerations of:

- 0.18 g at Cambria (Fig. 5)
- 0.12 g at San Antonio Dam
- 0.48 g at Templeton (Fig. 6)

All three stations are operated by the California Geological Survey (CGS) Strong Motion Instrumentation Program. Comparison of the records at Cambria (Fig. 5) and at Templeton (Fig. 6) show significantly higher accelerations and velocities at Templeton due to the directivity in rupture propagation. Data shows apparent strong directivity in the direction of the rupture propagation, from the epicenter toward the ESE (toward Templeton) (Boatwright & Seekins, 2004; Shakal et al., 2004).

The largest recorded shaking was at an instrumented 1-story hospital in Templeton, about 38 km SE of the epicenter (though much closer, about 16 km to the projected southern end of the rupture). The record at the 1st floor of the Templeton Hospital and response spectra compared to

UBC are shown in Figure 6 and 7. The response spectra in Figure 7 show that shaking was low energy, with strongest shaking exceeding UBC only at high frequencies. A peak value of 1.3 g was recorded at the roof of the hospital (1-story, wood-frame construction). Reports indicate little structural damage in the hospital, an important outcome. The ground level of the hospital is a good indication of the shaking in the vicinity, because the hospital is small and light.

After the earthquake a free field station (Templeton Hospital Ground) was reinstalled near the Templeton Hospital. Newly obtained records of 8 aftershocks at Templeton Hospital Ground demonstrate in average 1.37 (Standard Deviation $SD = 0.37$) higher peak ground acceleration than at the first floor of the hospital. Peak ground velocity was in average 1.18 higher ($SD = 0.20$). This suggests that most likely peak ground acceleration during the San Simeon earthquake in Templeton area was about 0.66 g with the corresponding peak ground velocity of about 39 cm/sec. Templeton is about 10 km from Paso Robles, where significant damage occurred.

Some of the next closest records are from the Parkfield area, with peak acceleration of 0.23 g at the Cholame 12W station (this station is closest to Paso Robles). The Parkfield Array, operated by CGS, recorded peak accelerations that ranged from 0.04 to 0.23 g, very similar to the range observed for the 1983 M 6.5 Coalinga earthquake.

Ground Motion Attenuation

A comparison of the peak acceleration data (103 data points) vs distance to the fault with that predicted by the Boore-Joyner-Fumal (BJF97, Boore et al., 1997) attenuation relationship is shown in Figure 8. The distances range from 12 km, for the Cambria station, to many stations at distances of over 250 kilometers. The data shows reasonable agreement with BJF97 in its applicable range. Coefficients for a reverse fault and an average shallow V_s of 700 m/sec were used; the thin line indicates distances beyond the suggested limit of the authors, 80 km. Beyond that, higher attenuation with distance than predicted by the extrapolated BJF97 curve is indicated. These new data, and other recent data from digital instruments, allow extending the existing relationships to greater distances.

The point above the BJF97 curve at about 16 km is Templeton, which had 0.48g, the largest value recorded in this earthquake; lying above the curve is consistent with directivity-increased shaking in the rupture direction. The two closest stations, Cambria and San Antonio Dam, both plot below the curve, consistent with directivity-reduced values in the direction away from the rupture.

Finite-Source Modeling

Finite-source modeling provides information about the length, width, average slip and when coverage is sufficient the detailed slip distribution and rupture kinematics (timing). These source parameters are important for better understanding source influences on near-fault strong ground motion. There are many different methods for the determination of this information. The method developed by Hartzell and Heaton (1983) has been used in various forms in numerous papers of the peer-reviewed literature, and today it is common to combine seismic, geodetic and

surface slip data to obtain greater constraint on the rupture process (e.g. Kaverina et al., 2002). Recently a method for the realtime determination of finite-source parameters was developed by Dreger and Kaverina (2000). A similar approach (Kuge et al. 2003) has been developed for Japan. The method outlined by Dreger and Kaverina (2000) was used to analyze strong ground motions recorded for the 22 December 2003 Mw6.5 San Simeon earthquake. The obtained finite-source information was used to update the ShakeMap the day of the earthquake compensating for the lack of near-fault observations of strong ground motions (Dreger et al., 2004).

For the past two years the Berkeley Seismological Laboratory has been operating a realtime finite-source method patterned after the approach outlined in Dreger and Kaverina (2000). Figure 9 illustrates the steps in this method. First a location and magnitude are determined from the dense short-period network operated by the USGS in Northern California. Second, if the local magnitude exceeds 3.4 then moment tensor software at the BSL is triggered to determine the scalar seismic moment, moment magnitude (M_w) and the focal mechanism. Third, if the event is greater than $M_w5.5$ finite-source inversions are performed to determine which of the nodal planes of the focal mechanism is the rupture plane, the dimensions of the rupture, the slip distribution and the rupture velocity. Details about how the fault model and the assumed rise time are scaled can be found in Dreger and Kaverina (2000). Very rapid line-source calculations and also plane-fault inversions are performed. The final step involves using the derived fault slip model to estimate the near-fault strong ground motions. In ShakeMap model estimates of ground motions from empirical relationships are used for interpolation purposes between the observations. Finite-source information can be used to adjust these empirical relations for directivity in a variety of waves, which include: 1) using source finiteness to calculate the distance to the closest point on the fault instead of to the epicenter, 2) using empirical attenuation relationships adjusted for directivity (e.g. Somerville et al., 1997), and 3) integration of the slip model to generate synthetic near-fault time histories which are then used to determine key ground motion parameters such as PGV, and S_a at 0.3, 1 and 3 seconds period.

The San Simeon earthquake provided the first test of this system, and the results are encouraging. Figure 10 shows the location of the earthquake, the surface projection of fault slip, and the locations of seismic stations and GPS deformation sites used to obtain the updated model. The seismic moment tensor and initial finite-source model for the San Simeon earthquake determined on the day of the earthquake has been published in Hardebeck et al. (2004). The finiteness determined from the analysis described above was used to update the published ShakeMap the day of the event. Figure 11 compares several instrumental intensity (e.g. Wald et al., 1999) ShakeMaps for the event. The top left panel shows the ShakeMap produced with the available M_w . This map suffers from a lack of stations and is therefore controlled by estimated ground motions from empirical attenuation relations and site corrections. The top right panel shows the map in which the finite-source information was used to adjust the distance measure so that it was to the closest point to the fault. The finite-source modeling described below indicated that the event extended about 25 km to the SE of the epicenter (shown as the thick line on the ShakeMap). This addition greatly increased the area of large instrumental intensity and also shifted large instrumental intensity to the SE to Paso Robles consistent with where most of the damage was concentrated. Directivity also played an important role in the elevation of ground motions to the SE. The finite-source model used to infer source dimensions for ShakeMap on the day of the earthquake is published in Hardebeck et al. (2004).

The current ShakeMap is shown in the bottom right panel. In this map the finite-source extent and also near-fault strong motion observations were combined. This map compares closely with the initial finite-source map (without near-fault observations, top right) and the final map without the finite-source constraint (bottom left). Thus the addition of finite-source information at a time when near-fault strong motion recordings were not yet available resulted in a ShakeMap much closer to the truth than the initial map without the data. It is notable that even with the near-fault strong motion stations the finite-source extent contributes significantly to the ShakeMap and likely gives a truer estimate of the near-fault shaking given the relatively sparse instrumental coverage.

We have refined the finite-source model for the event by incorporating additional seismic stations, adding GPS deformation data, and testing the rupture velocity and rise time parameter space. The updated model shown in Figure 12 is for a rupture velocity of 2.6 km/s and utilizes 6 time windows following the method of Hartzell and Heaton (1983) to account for rupture velocity and rise time variability during the rupture process. As Figure 12 shows the slip is generally shallower than the hypocenter with the peak slip occurring in the 8 to 4 km range. The lateral extent of slip is much greater with a total length of about 30 km to the SE of the hypocenter inferred from the model. This is an unusual slip aspect ratio for a dip-slip earthquake. Figure 13 shows the fit to the seismic waveform data, which is found to be very good, and as shown on Figure 10 the fit to the GPS data is also very good. Using this slip model the velocity time histories for Templeton, CA site were simulated and are compared to the observations in Figure 14. The rock synthetics were site adjusted for the low surficial velocities at the Templeton station. Although Templeton was not used to derive the slip distribution the predicted motions compare very favorably with the observations in terms of both peak amplitudes and waveform.

The derived slip distribution was also used to compute a synthetic rock motion peak ground velocity (PGV) ShakeMap which is shown in Figure 15a for the actual model, and in Figure 15b for a model assuming that the slip occurred on a vertical strike-slip fault. This simulation shows that while directivity in the San Simeon earthquake was indeed important in elevating the ground motions to the SE of the epicenter and ruptured fault, the directivity was relatively mild. The hypothetical vertical strike-slip earthquake would have produced peak velocities as much as a factor of three larger at some sites, extended the region of high ground velocity (greater than 10 cm/s) tens of kilometers further to the SE, and increased the ground area experiencing greater than 10 cm/s peak velocity 4-fold.

Results

A comparison of the peak ground acceleration vs distance to the fault with that predicted by the BJF97 attenuation relationship shows reasonable agreement in its applicable range. Beyond 80 km from the fault, higher attenuation with distance than that predicted by the extrapolated BJF97 curve is indicated. These new data, and other recent data from digital instruments, allow extending the existing relationships to greater distances.

Significant directivity in ground motion due to rupture propagation to southeast toward Paso Robles & Templeton was observed in strong motion data, and matches concentration of damage SE of the epicenter.

The combined inversion of GPS and seismic waveform data for the kinematic rupture process of the San Simeon earthquake reveals an elongated rupture over a narrow, shallow depth range. While directivity was also a factor in the strength of the ground motions comparative simulations between the deep-slip case and a hypothetical strike-slip case reveals that a $M_w 6.5$ strike-slip event with identical slip distribution would result in about 3-4 times increase in PGV.

Acknowledgements

The authors highly appreciate contribution of A. Shakal, M. Huang, H. Haddadi, K.W. Lin, C. Petersen, A. Cramlet and P. Roffers. Douglas Dreger would like to acknowledge support received from the USGS, PG&E and the CEC through the PEER lifelines program to develop the automated finite-source method.

References

- Boatwright J., Seekins L.C. (2004). Directivity in the near-field and regional recordings of the 22 December 2003 San Simeon earthquake. *Seismological Research Letters*. V. 75, No. 2, 265.
- Boore, D. M., W. B. Joyner and T. E. Fumal (1997). Equations for estimating horizontal response spectra and peak acceleration from western North American earthquakes: A summary of recent work. *Seismological Research Letters*. V. 68, No. 1, 128-153.
- Dreger, D. S. and A. Kaverina (2000). Seismic remote sensing for the earthquake source process and near-source strong shaking: a case study of the October 16, 1999 Hector Mine earthquake, *Geophys. Res. Lett.*, 27, 1941-1944.
- Dreger, D. S., P. Lombard, J. Boatwright, D. J. Wald and L. S. Gee (2004). Finite source models of the 22 December 2003 San Simeon earthquake and applications to ShakeMap, *Seismo. Res. Lett.*, 75, 293.
- Gee L., Oppenheimer D., Shakal T., Given D., Hauksson E. (2004). Performance of the CISN during the 2003 San Simeon earthquake. CISN Report at http://www.cisn.org/docs/CISN_SanSimeon.pdf
- Hardebeck J.L., Boatwright J., Dreger D., Goel R., Graizer V., Hudnut K., Ji C., Jones L., Langbein J., Lin J., Roeloffs E., Simpson R., Stark K., Stein R., and J. Tinsley (2004). Preliminary report on the 22 December 2003, M 6.5 San Simeon, California Earthquake. *Seismological Research Letters*. V. 75, No. 2, 155-172.
- Hartzell, S. H., and T. H. Heaton (1983). Inversion of strong ground motion and teleseismic waveform data for the fault rupture history of the 1979 Imperial Valley, California, earthquake, *Bull. Seism. Soc. Am.*, 73, 1553-1583.

Hauksson E., Oppenheimer D. (2004). Preliminary 3D Vp model for the 2003 M_w 6.5 San Simeon mainshock – aftershock region. *Seismological Research Letters*. V. 75, No. 2, 265.

Jennings C.W. (1994). Fault activity map of California and adjacent areas, with locations and ages of recent volcanic eruptions. *California Division of Mines and Geology, Geologic Data Map No. 6, map scale 1:750,000*.

Kaverina, A., D. Dreger, and E. Price (2002). The combined inversion of seismic and geodetic data for the source process of the 16 October, 1999, Mw7.1 Hector Mine, California, earthquake, *Bull. Seism. Soc. Am.*, 92, 1266-1280.

Kuge, K. (2003). Source modeling using strong-motion waveforms: toward automated determination of earthquake fault planes and moment-release distributions, *Bull. Seism. Soc. Am.*, 93, 639-654.

Shakal A., Graizer V., Savage W., Stephens C. (2004). Preliminary analysis of strong-motion data from the M 6.5 San Simeon earthquake of 22 December 2003. *Seismological Research Letters*. V. 75, No. 2, 265.

Treiman J.A, Tinsley J.C., Rosenberg L.I., Keefer D.K, Knudsen K.I., Loyd R.C., Manson M.W., McCrink T.P., Reid M.E., Schmidt K., Wilson R.I. (2004). Surface effects of the 22 December 2003 Mw 6.5 San Simeon earthquake. *Seismological Research Letters*. V. 75, No. 2, 264.

Wald, David J., Vincent Quitoriano, Thomas H. Heaton, Hiroo Kanamori, Relationships between Peak Ground Acceleration, Peak Ground Velocity and Modified Mercalli Intensity in California, *Earthquake Spectra*, **15**, 557-564



Figure 1. CISN strong-motion stations in San Simeon area.

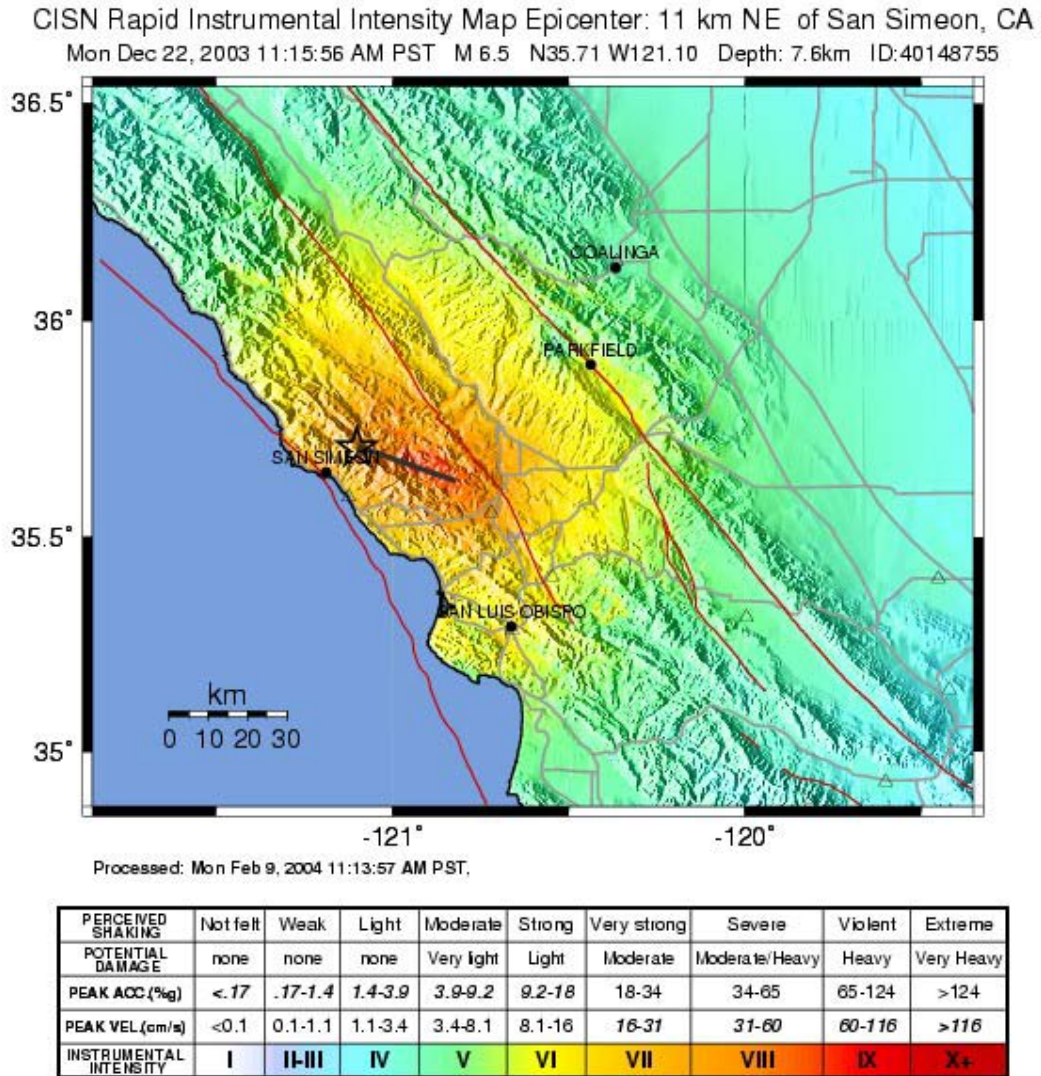


Figure 2. Instrumental Intensity ShakeMap for the M6.5 San Simeon earthquake.

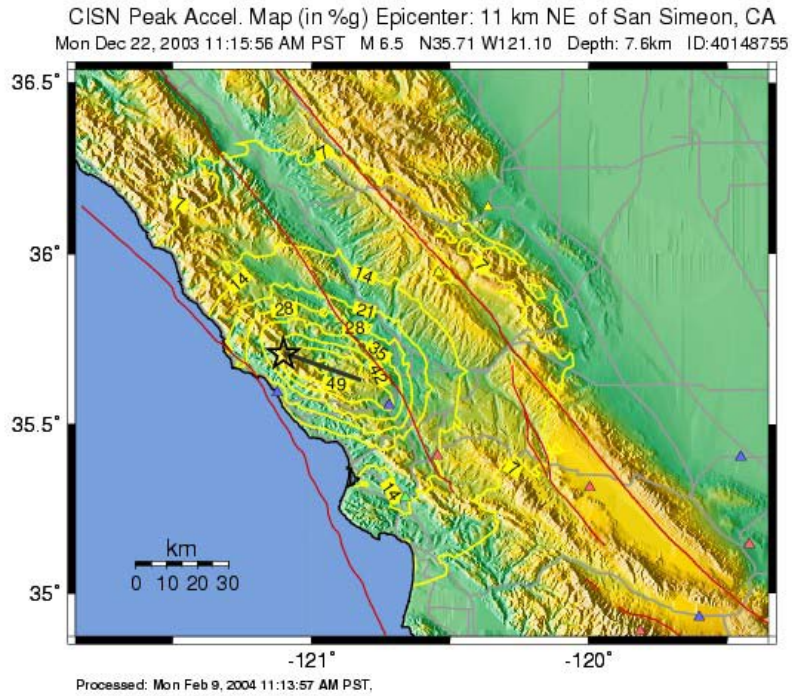


Figure 3. Peak ground acceleration ShakeMap for the San Simeon earthquake.

San Simeon Earthquake of 22 Dec 2003, 11:15:56 AM PST, 6.5Mw - Microsoft Internet Explorer

Address: http://www.quake.ca.gov/cisn-ed/IQR/SanSimeon_22Dec2003/iqr_dist.htm

CISN Internet Quick Report
 Strong-Motion Data Set For

San Simeon Earthquake of 22 Dec 2003
 6.5 ML, 11:15:56 AM PST, 35.706N 121.102W Depth 7.6km.

Earthquake Information: [Update/Data Highlights](#) [Hypocenter](#) [ShakeMap](#)

Stations listed in increasing **Epicentral Distance** (Alternatively, select [alphabetical listing](#))

Table Last Updated: 05 Apr 2004 12:37

Station Name	Station No./ID	Network	Dist. (km)	Horiz Apk (g)		View	Download
				Ground	Struct.		
Cambria - Hwy 1 Caltrans Bridge Grnds	37737	CGS	13	.179	--	<input type="radio"/>	<input type="radio"/>
San Antonio Dam	36258	CGS	22	.12	.22	<input type="radio"/>	<input type="radio"/>
Templeton - 1-story Hospital	36695	CGS	38	.483	1.28	<input type="radio"/>	<input type="radio"/>
Parkfield - Vineyard Canyon 6W	36441	CGS	49	.09	--	<input type="radio"/>	<input type="radio"/>
Point Buchon - Los Osos	36427	CGS	52	.089	--	<input type="radio"/>	<input type="radio"/>
Parkfield - Vineyard Canyon 5W	36440	CGS	52	.06	--	<input type="radio"/>	<input type="radio"/>
Parkfield - Vineyard Canyon 4W	36446	CGS	55	.04	--	<input type="radio"/>	<input type="radio"/>
Parkfield - Vineyard Canyon 3W	36176	CGS	57	.09	--	<input type="radio"/>	<input type="radio"/>
Parkfield - Vineyard Canyon 2W	36447	CGS	59	.07	--	<input type="radio"/>	<input type="radio"/>
Parkfield - Fault Zone 15	36445	CGS	61	.06	--	<input type="radio"/>	<input type="radio"/>
San Luis Obispo - Rec Ctr	01083	USGS	62	.165	--	<input type="radio"/>	<input type="radio"/>
Parkfield - Fault Zone 9	36443	CGS	62	.08	--	<input type="radio"/>	<input type="radio"/>
Parkfield - Fault Zone 14	36456	CGS	62	.09	--	<input type="radio"/>	<input type="radio"/>
Parkfield - Vineyard Canyon 1E	36455	CGS	63	.10	--	<input type="radio"/>	<input type="radio"/>

Figure 4. CISN Internet Quick Report for the San Simeon earthquake.

SMIP04 Seminar Proceedings

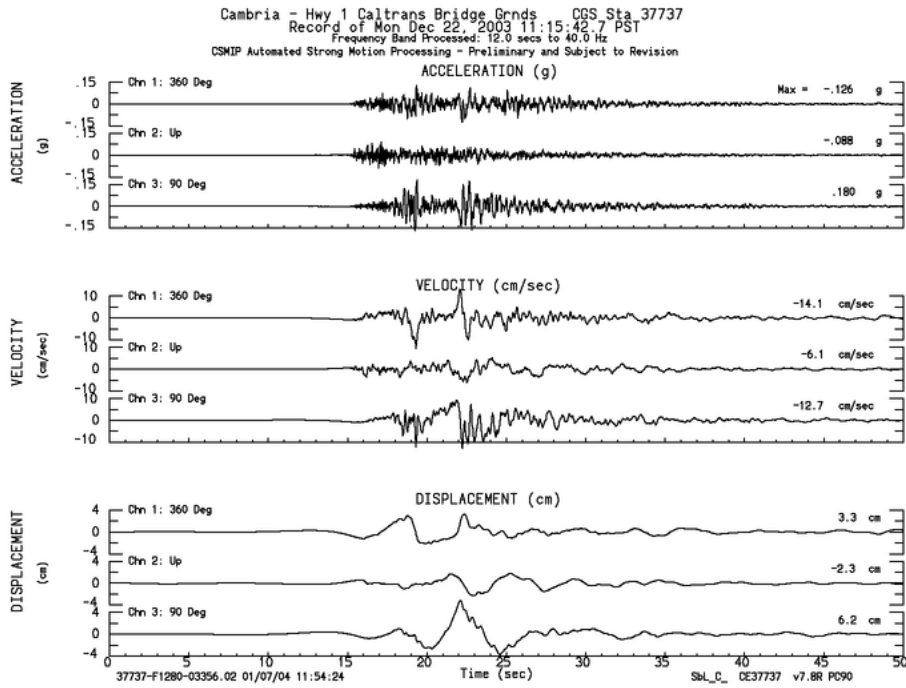


Figure 5. Acceleration, velocity and displacement recorded in Cambria during the San Simeon earthquake.

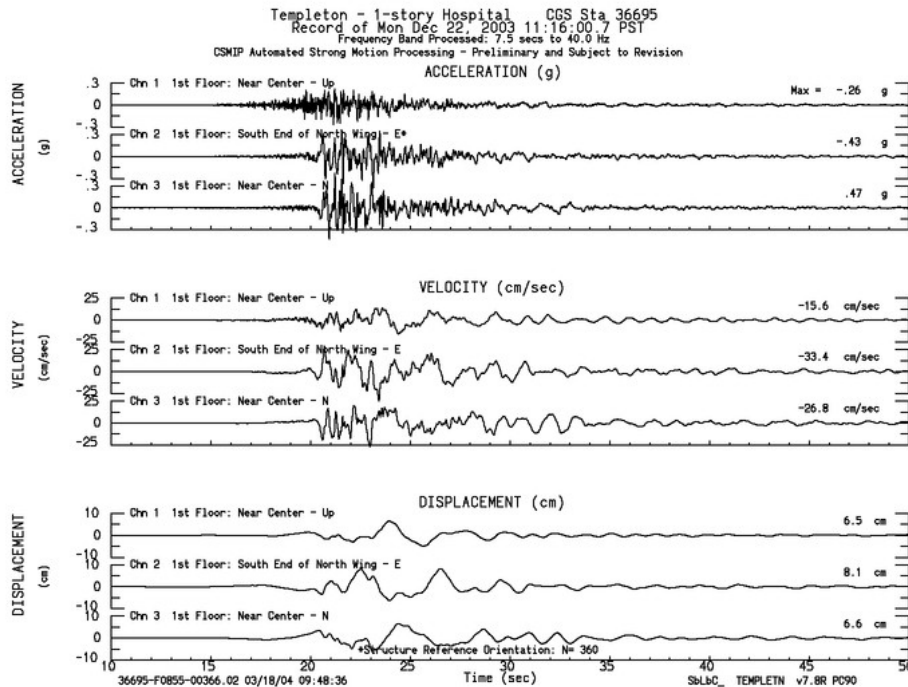


Figure 6. Acceleration, velocity and displacement recorded at the 1st floor of the one-story Templeton Hospital.

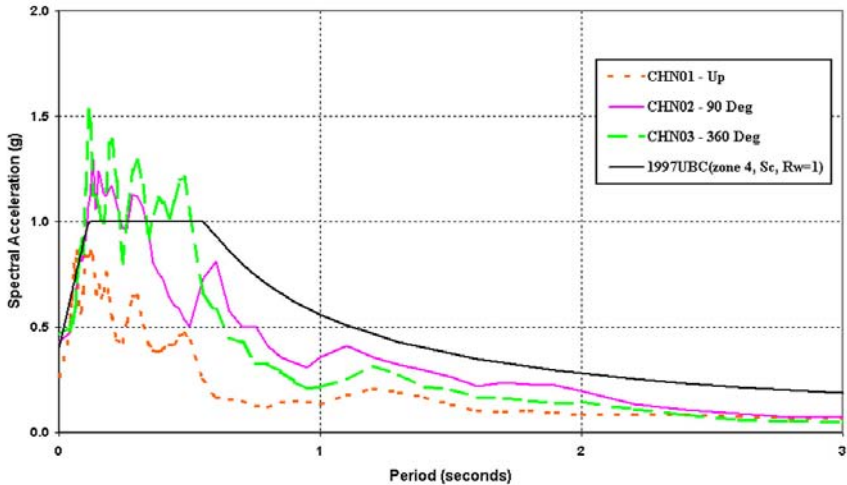


Figure 7. 5% damped response spectra for the 1st floor channels of the Templeton Hospital compared to the Universal Building Code (UBC). Figure courtesy of M. Huang.

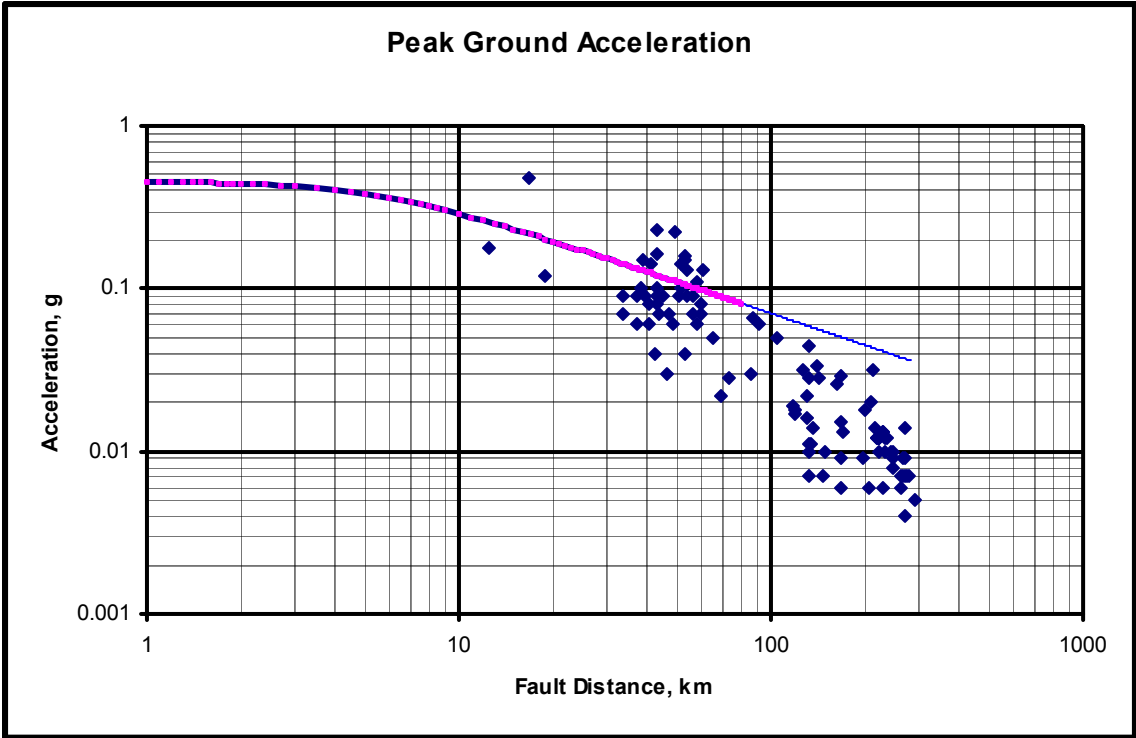


Figure 8. Peak horizontal ground acceleration data plotted against the distance to the fault, and the Boore-Joyner-Fumal (BJF97, Boore et al., 1997) attenuation relationship. The data shows reasonable agreement with BJF97 in its applicable range of 80 km. Beyond that, higher attenuation with distance than predicted by the extrapolated BJF97 curve is indicated (the thin line indicates distances beyond the suggested limit of the authors).

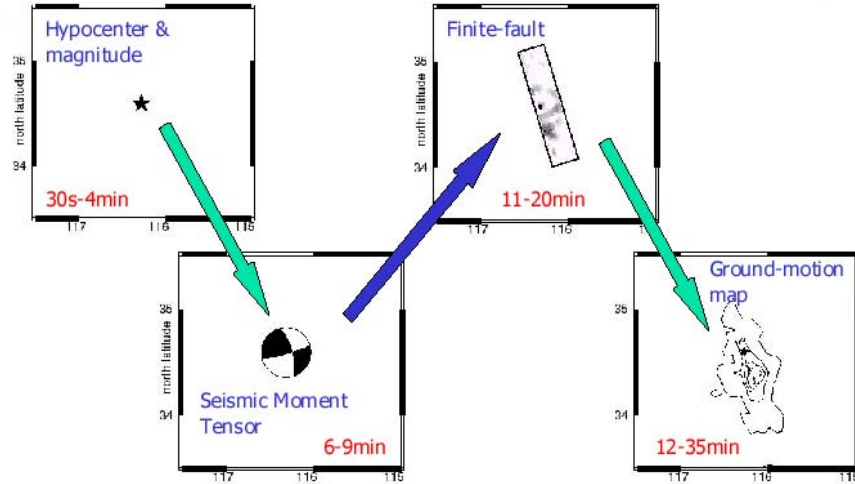


Figure 9. Illustration of automatic processing system at Berkeley. The times shown are elapsed time from the event origin time. In the last panel near-fault ground motions are simulated from the slip distribution.

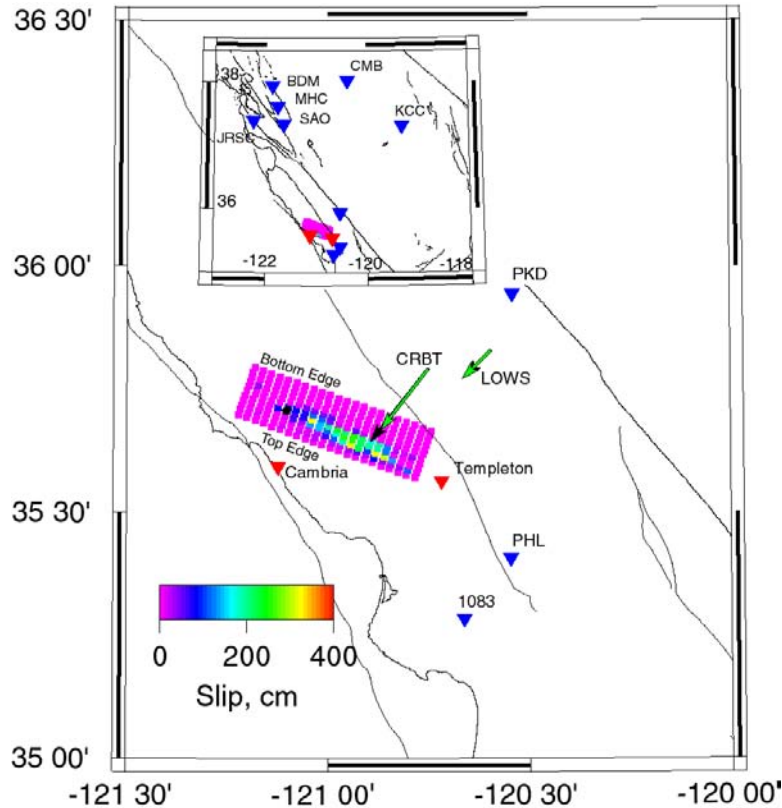


Figure 10. Location map and map-view projection of fault slip. The epicenter is marked by the black circle. Seismic stations used to determine the fault slip are shown as the blue inverted triangles. The red inverted triangles are for sites that have been used to test forward predictions of ground motions from the derived model. Observed GPS deformation (black arrow) at two near-fault sites are compared to predictions (green arrows) from the model. Slip extends about 30 km to the SE toward Templeton and Paso Robles. This source finiteness and a SE directivity contributed to the large motions recorded at Templeton and the damage at Paso Robles.

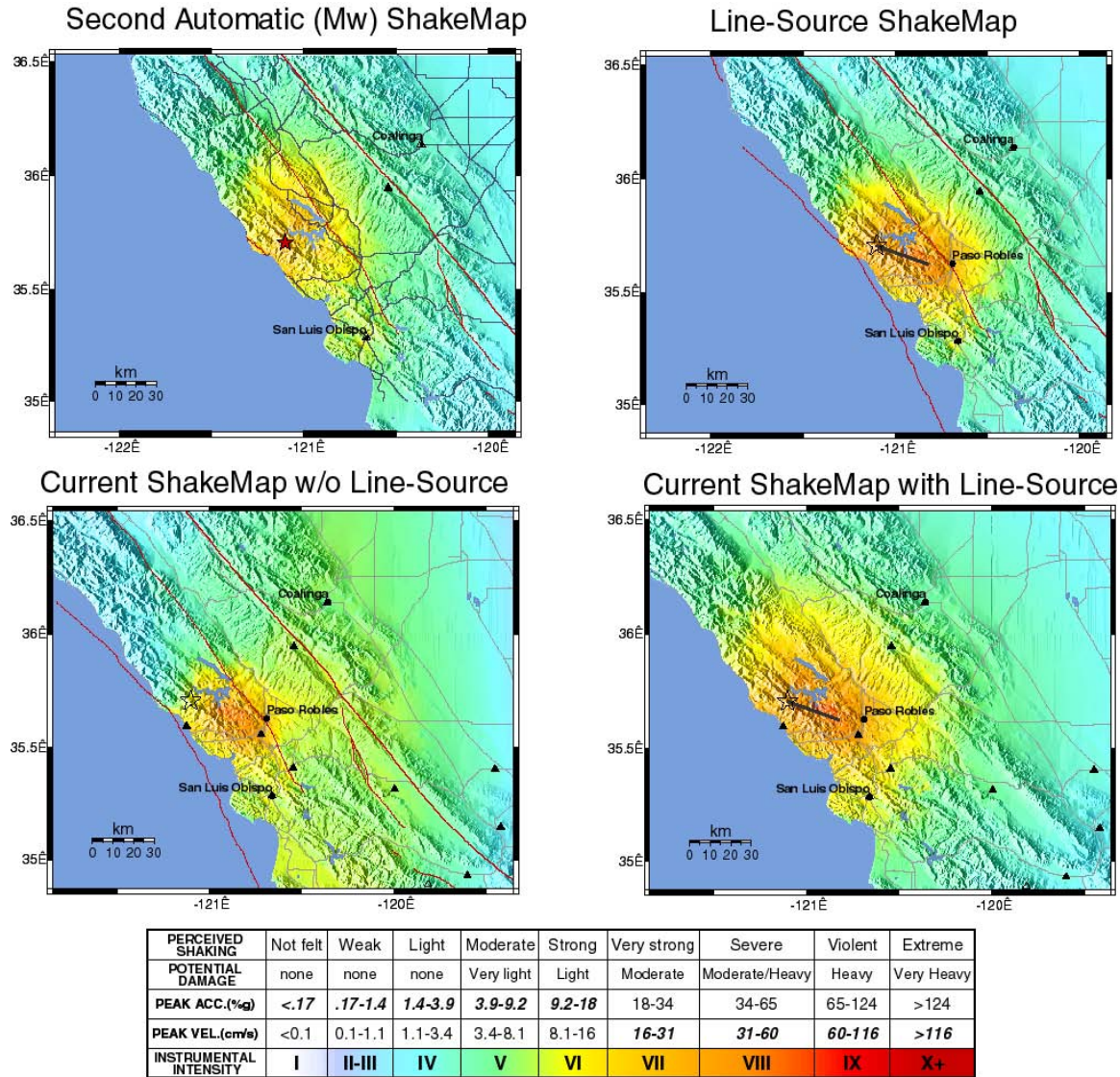


Figure 11. Automatic instrumental intensity ShakeMap (top left). Finite fault adjusted ShakeMap (top right). The line shows the extent of fault rupture used to calculate the distance to the fault in the calculation of the ShakeMap. Note the lack of near-fault, realtime strong motion stations in the affected area. The most up to date ShakeMap (current map), which includes available near-fault ground motion values is shown in the lower right panel. The lower left panel shows the current map without the source finiteness component. A comparison of the top right and lower left panels illustrates that the addition of finite-source information greatly improved the ShakeMap in the near-fault and damage zones in the absence of near-fault ground motion information. Furthermore the finite-source adjusted map is a much truer estimate of ground motion than the automatic map based only on Mw, distant recordings and empirical ground motion estimates.

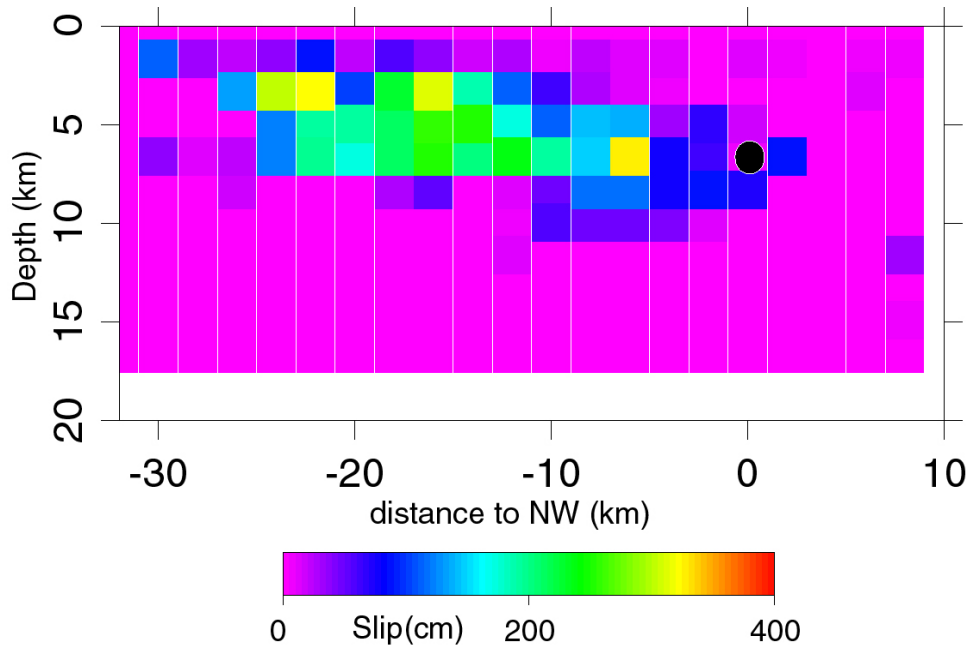


Figure 12. Fault slip. Slip is shallower than the hypocenter (black circle), peaked in the 8 to 3 km depth range, and extends 25 km to the SE of the hypocenter.

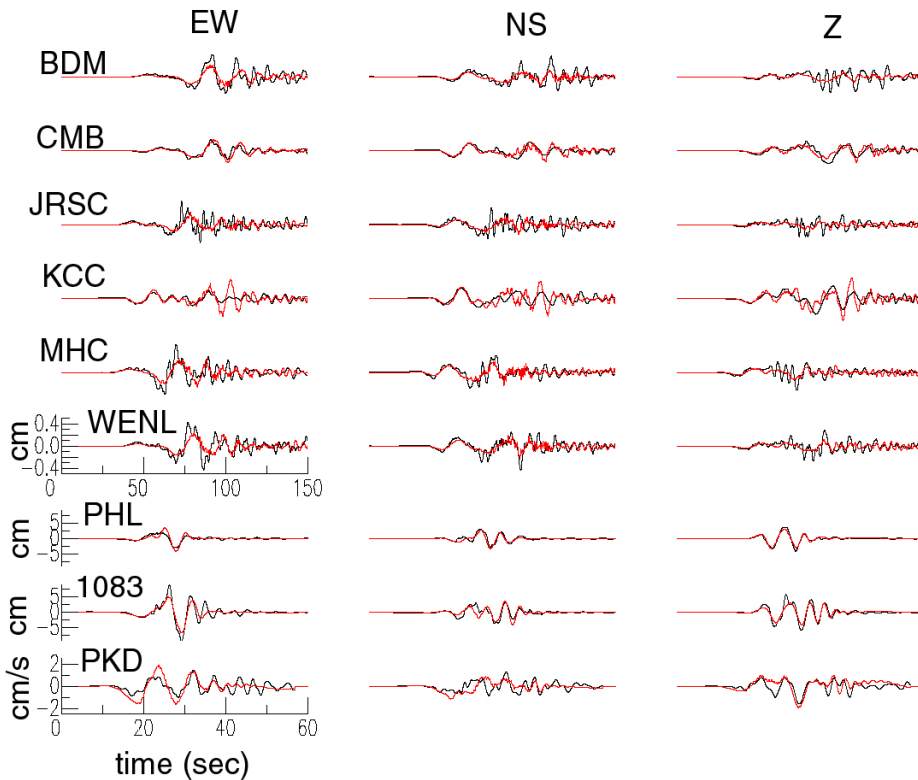


Figure 13. Observed displacement and velocity (black traces) are compared to synthetics (red traces) constructed for the model shown in Figure 4. The data and synthetics are broadband with a high pass filter at 0.01 Hz and a nyquist frequency of 5 Hz.

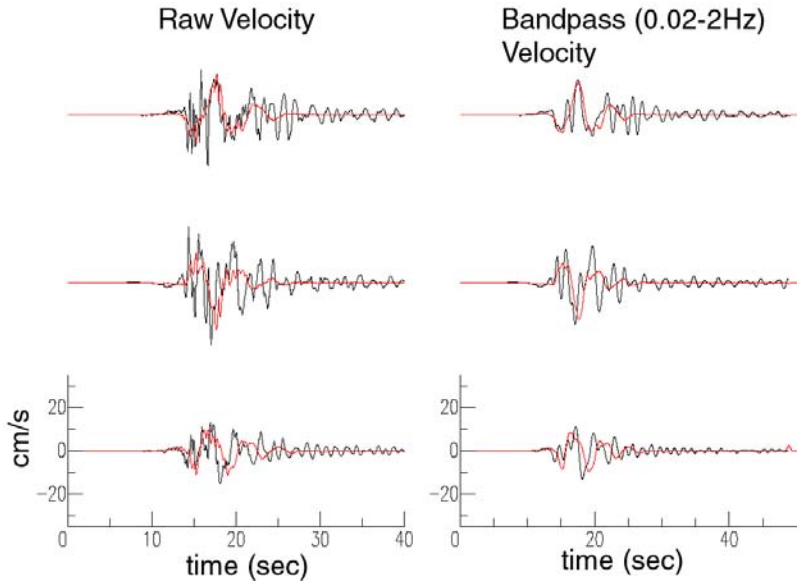


Figure 14. Observed (black) and predicted (red) ground velocity at the Templeton site. The hard rock synthetics were site-corrected.

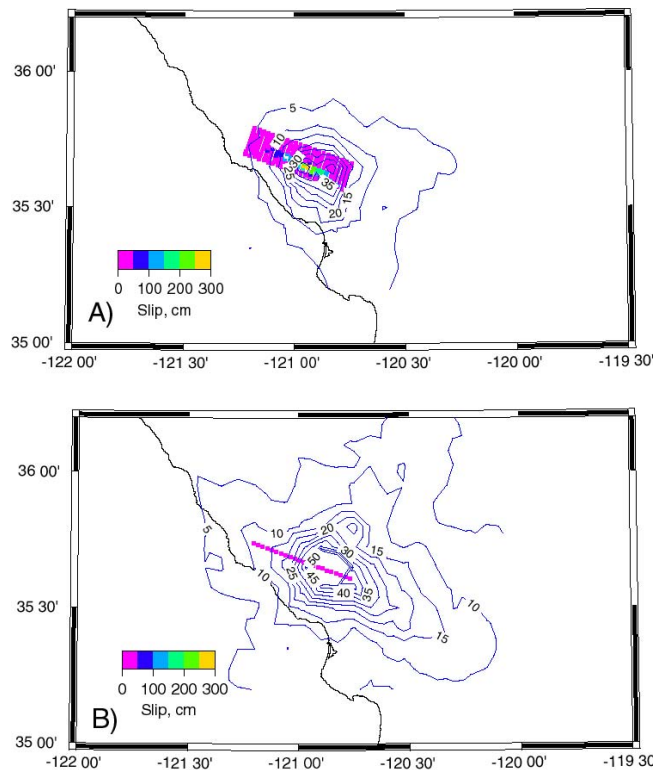


Figure 15. Simulated peak ground velocity in cm/s for the San Simeon earthquake slip model (a), and a hypothetical vertical strike-slip fault (b). In each case an identical slip distribution and slip time history was assumed. The only difference is the orientation of the plane and the direction of the slip (perpendicular to strike in (a), and parallel to strike in (b)). The Green's functions that were used is for a represented hard rock model for the region. This plot illustrates that the laterally extending dip-slip rupture of the San Simeon earthquake produces a relatively mild directivity effect compared to a vertical strike-slip fault in the same place.